JNM The Journal of NUCLEAR MEDICINE

2014 SNMMI Highlights Lecture: Oncology

J Nucl Med. 2014;55:9N-24N.

The Journal of Nuclear Medicine is published monthly.
SNMMI | Society of Nuclear Medicine and Molecular Imaging
1850 Samuel Morse Drive, Reston, VA 20190.
(Print ISSN: 0161-5505, Online ISSN: 2159-662X)

SNMMI SOCIETY OF NUCLEAR MEDICINE AND MOLECULAR IMAGING

2014 SNMMI Highlights Lecture: Oncology

From the Newsline Editor: The Highlights Lecture, presented at the closing session of each SNMMI Annual Meeting, was originated and presented for more than 33 years by Henry N. Wagner, Jr., MD. Beginning in 2010, the duties of summarizing selected significant presentations at the meeting were divided annually among 4 distinguished nuclear and molecular medicine subject matter experts. The 2014 Highlights Lectures were delivered on June 11 at the SNMMI Annual Meeting in St. Louis, MO. The neuroscience presentation was included in the September Newsline issue and the cardiovascular imaging presentation in the October issue. In this issue we feature the lecture by Umar Mahmood, MD, PhD, who spoke on highlights in oncology. Note that in the following presentation summary, numerals in brackets represent abstract numbers as published in The Journal of Nuclear Medicine *(2014;55[suppl 1]).*

Oncology presentations at this meeting included 252 basic science reports and 276 clinical reports—far too many to review in the limited time allotted for these highlights. One of the highlights for me was listening to the Cassen Lecture, titled "What Have We Learned from the National Oncologic PET Registry," delivered by this year's Cassen awardee, Barry A. Siegel, MD, reviewing what we have done and can do as a community to advance patient care in cancer.

Scientific knowledge about cancer is accelerating in terms of understanding mechanisms of disease, cancer pathways, and the cell types involved. It is encouraging that the imaging sciences are keeping pace with this acceleration of discovery, and we saw many of these innovations highlighted at this SNMMI meeting.

It may seem a little trite in an overview of oncology to show slides from Hanahan and Weinberg's "Hallmarks of cancer: the next generation" (*Cell*. 2011;144:646), but at this meeting we heard presentations on imaging of cells throughout the tumor microenvironment, including immune cells, cancer stem cells, endothelial cells, and invasive cancer cells as they change from epithelial to mesenchymal phenotypes. With increased specificity of therapeutic targeting of different cancers we are able to image receptor tyrosine kinases to help guide therapy choices, for example, guiding inhibition of epidermal growth factor receptor (EGFR) when it is overexpressed. We are looking at proliferation to study cyclin-dependent kinase inhibitors. We are looking at immune cell activation by imaging immune cells and at vascular changes by documenting vascular endothelial growth factor (VEGF) signaling. We are researching metabolic changes, for example, with aerobic glycolysis inhibitors. For all of these fundamental hallmarks of cancer, we are engaged in continuous enhancement of techniques and expansion of knowledge to improve imaging for diagnosis and to guide therapeutic decision making.

Complementary Cell-Based Assays

Laura Sasportas, PhD, from Stanford University (CA), received the Young Investigator Award from the Nuclear Oncology Council. With Stanford colleagues, she reported on "Single-cell metabolomics in circulating tumor cells" [8]. These researchers developed a way to look at the amount of ^{18}F-FDG uptake in individual cancer cells, using an orthotopic imageable mouse model of metastatic breast cancer, in which tumor cells were labeled with green fluorescent protein. Circulating tumor cells were then pulled out for single-cell autoradiography and radioluminescence microscopy. The resulting data on ^{18}F-FDG uptake per cell in the primary tumor showed that certain clones in the circulating tumor cells have much higher uptake. This raises the question of whether this phenotype predisposes to metastasis. As is well known, many cancer cells are seen in circulation, but very few lead to metastasis. It will be interesting to learn more about the ways in which this phenotype correlates with properties such as eventual metastasis.

Umar Mahmood, MD, PhD

Guruswami et al. from Washington University School of Medicine (St. Louis, MO) reported on "Assessment of P-glycoprotein (Pgp; ABCB1)–mediated functional transport in human epidermal carcinoma cells using live cell imaging: Impact of overall charge on Pgp recognition profiles" [340]. These authors developed a fluorescent probe for this application, with results suggesting that it might be possible to screen for multidrug resistance through the Pgp using circulating tumor cells. These approaches complement imaging techniques that provide whole-body information by, in this case, offering the possibility of a simple serum test to act as an adjunct to imaging.

In Vivo Targeted Imaging/Therapeutic Probes in Murine Models

Cancer cells can transform from standard epithelial phenotypes to mesenchymal phenotypes, where they become more amoeboid, begin migrating more, and then metastasize more. Yang et al. from the University of Wisconsin–Madison reported on "ImmunoPET imaging of CD146, a novel epithelial-mesenchymal transition (EMT) marker" [1]. This group nicely showed that they can image this transformation using ^{64}Cu-NOTA-YY146 PET/CT in mice (Fig. 1). This type of imaging can be used to characterize tumors in situ as well as at different metastatic sites.

Yang et al. from TRIUMF and the British Columbia Cancer Agency (Vancouver, Canada) and GE Global Research (Niskayuna, NY) reported on "Oxidative stress imaging in triple-negative breast cancer using a cystine transporter tracer [^{18}F]5-fluoro aminosuberic acid (FASu)" [4]. We have seen that different probes are being used to assess the cysteine transporter, which is a potential marker

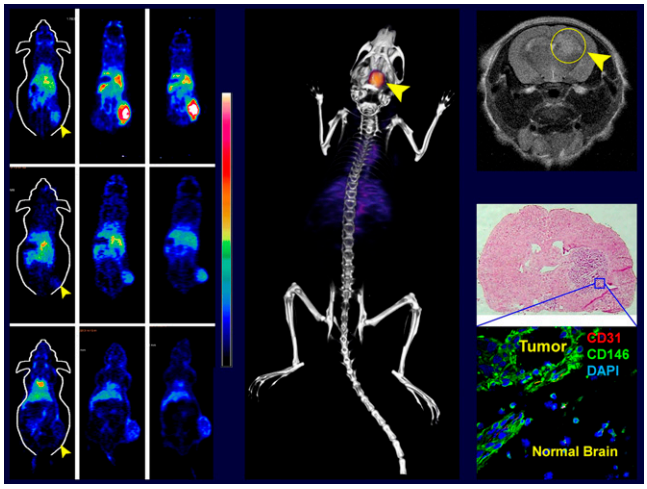

FIGURE 1. Imaging with ^{64}Cu-NOTA-YY146 for imaging epithelial-mesenchymal transition. Left block: ^{64}Cu-NOTA-YY146 PET images in mice. Top: U87MG; middle: U87MG plus blocking; bottom: PC3. U87MG cells are CD146-positive and PC-3 cells are CD146-negative. Middle block: PET/CT of orthotopic U87MG. Right block: Top: T2-weighted MR imaging; middle: histology; bottom: autoradiography showing tumor and normal cells.

of oxidative stress. These probes can be helpful at optimizing cancer therapies by assessing how different types of cells live under stressful conditions. In this case, the researchers tested their PET probe in mice and were able to successfully image specific tumors (Fig. 2). Their results indicated that the presence and function of the cysteine transporter caused an increase in ^{18}FASu uptake in breast cancer cells, suggesting that the cysteine transporter might be a viable alternative PET biomarker of oxidative stress in vivo.

Another example of oxidative stress imaging came from Lee et al. from Asan Medical Center at the University of Ulsan College of Medicine (Seoul, Republic of Korea) and Piramal Life Sciences (Berlin, Germany), who reported that "(4S)-4-(3-[^{18}F]fluoropropyl)-L-glutamate (^{18}F-FSPG) uptake correlates with cancer stem cell (CSC) markers in cancer patients" [548]. One interesting result from this work suggested that CSCs will also have increased levels of this system xc-transporter activity. They have used this probe in humans, and their data indicated that ^{18}F-FSPG uptake correlates with the expression of a subset of CSC markers, that ^{18}F-FSPG uptake does not show significant correlation with epithelial–mesenchymal transition markers, and that ^{18}F-FSPG uptake may be one of the manifestations of the CSCs.

One way we can advance individualized therapy is to use imaging to help tailor dosing to specific patient characteristics. Heidari et al. from the Massachusetts General Hospital (Boston) reported that "^{18}F-fluoroestradiol PET guides dosing of selective estrogen receptor degraders" [11]. These researchers showed in histologic analyses that as drug levels increased estrogen receptor levels decreased, but proliferation had not yet changed. With PET/CT in xenografts they showed that it is possible to monitor the level of estrogen receptor after different doses of therapy, even before ^{18}F-FDG changes are evident (Fig. 3). As we begin to integrate more individualized treatment paradigms into routine clinical work, we will be able to use imaging data to help guide choices in dosage.

Another presentation on pharmacodynamic imaging came from Lee et al. from Gachon University (Incheon, Republic of Korea) and Asan Medical Center at the University of Ulsan College of Medicine (Seoul, Republic of Korea), who reported on "PET imaging of human colon cancer xenografts in mice with [^{18}F]fluorothymidine (^{18}F-FLT) after TAS-102 treatment" [334]. TAS-102 is an orally administered agent under development for colorectal cancer treatment. It is composed of a thymidine phosphorylase inhibitor and α,α,α-trifluorothymidine, which has a similar structure to ^{18}F-FLT. In this case, when the drug was active, the level of ^{18}F-FLT uptake increased, suggesting successful

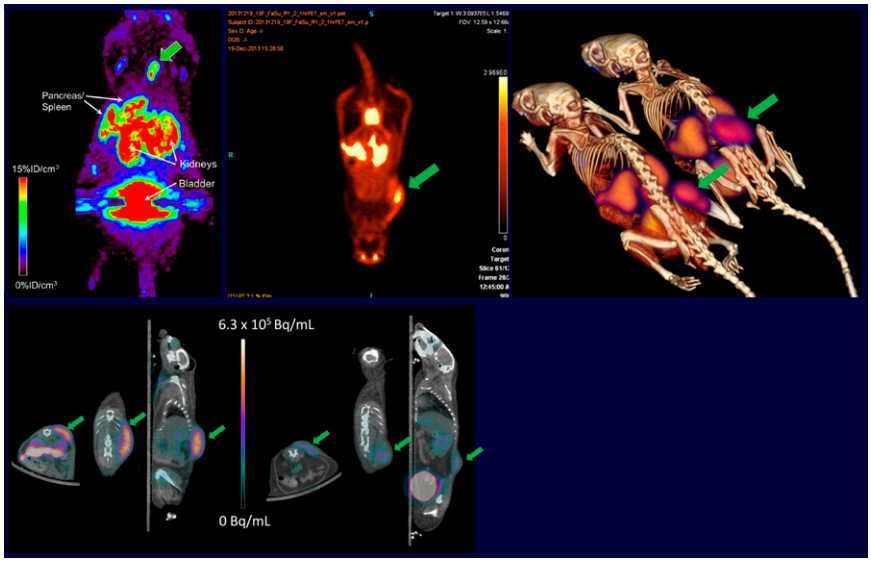

FIGURE 2. MicroPET imaging with ^{18}FASu in different animal strains for assessing oxidative stress. Top (left to right): Uptake in SKOV3 tumor at 1 hour after injection in a CD1 nude mouse; uptake in MDA MB-231 tumor at 1 hour after injection in an NOD/SCID mouse; and uptake in EL4 tumors 2 hours after injection in RAG2M mice. Bottom: Green arrows in left images show EL4 tumor uptake. Green arrows in right images show ASu blocking.

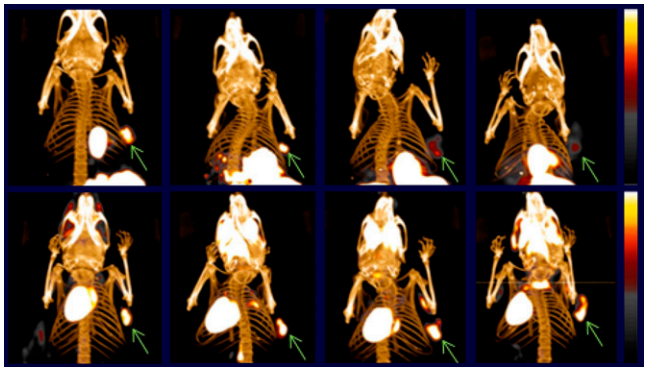

FIGURE 3. ^{18}F-FES and ^{18}F-FDG PET/CT in MCF-7 xenografts demonstrates changes in estrogen receptor levels prior to changes in metabolism. Top row: ^{18}F-FES PET/CT with (left to right) vehicle, 0.05, 0.5, and 5 mg fulvestrant. Bottom: ^{18}F-FDG PET/CT with (left to right) vehicle, 0.05, 0.5, and 5 mg fulvestrant.

response. The researchers showed this in mouse models, where they observed a biphasic response, with early uptake increases when the drug was successful, followed by decreases in uptake. This "flare" of ^{18}F-FLT uptake was identified as a marker of response to this therapy targeting a specific proliferation pathway.

A number of multimodality imaging agents were presented at this meeting. Muselaers et al. from Radboud University Medical Center (Nijmegen, The Netherlands) reported on "Radionuclide and fluorescence imaging of renal cell carcinoma using dual-labeled anti-carbonic anhydrase IX antibody G250" [66]. This group visualized renal cell carcinoma with both SPECT/CT and near-infrared imaging, specifically for preoperative guidance. Images in mice showed successful pinpointing of tumor for margin-sparing surgery (Fig. 4), with promise for clinical applications, such as in nephron-sparing surgery. The authors are currently planning to extend these studies in a phase 1 clinical trial with the dual-modality tracer ^{111}In-G250-IRDye800CW to assess the feasibility of image-guided surgery in patients with clear cell renal cell carcinoma.

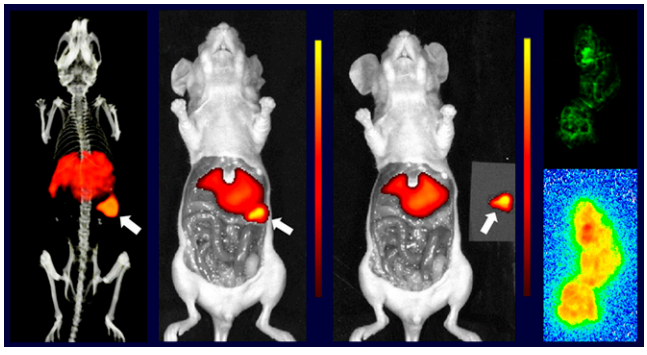

FIGURE 4. SPECT/CT and near-infrared (NIR) renal imaging with ^{111}In-G250-IRDye800CW targeting carbonic anhydrase IX. Left to right: SPECT/CT, NIR imaging, and NIR imaging postsurgery. Far right: Top, ex vivo NIR; bottom, ex vivo autoradioradiography.

Nanoparticles are another area of prolific research interest. Chen et al. from the University of Wisconsin–Madison reported on "A multifunctional CuS@MSN nanoplatform for tumor-targeted PET imaging, drug delivery, and photothermal therapy" [168]. These researchers developed mesoporous nanoparticles (MSNs) that can be labeled with ^{64}Cu for PET imaging and with fluorochromes for optical imaging, as well as loaded with drugs for delivering therapeutics at a higher dose to tumors. The researchers targeted CD105, an endothelial marker in new tumor vasculature. Resulting images showed high uptake with this targeting, with potential as both a diagnostic agent to visualize accumulation at the target site and as an agent for monitoring drug delivery, which could include radioactive or nonradioactive therapies (Fig. 5).

Lu et al. from the University of Connecticut (Storrs) and Hartford Hospital (CT) reported on "Intraperitoneal delivery of radiotherapeutic MSNs as a treatment for peritoneal tumor metastases" [210]. MSNs containing stable ^{165}Ho were synthesized with mean sizes of 60 and 120 nm and subsequently activated in a neutron flux to produce ^{166}Ho-MSNs. Regardless of size, focal accumulation of MSNs in tumors 24 h after intraperitoneal administration was observed in a variety of peritoneal metastatic ovarian (SKOV-3, OVCAR-8, NCI-ADR/RES) and pancreatic (MIA PaCa-2) tumor models. Tumor accumulation of these MSNs was observed to increase after 1 week. MSNs migrated from the surface to significant tumor depths over time as evidenced by autoradiography, optical imaging, and confocal microscopy of

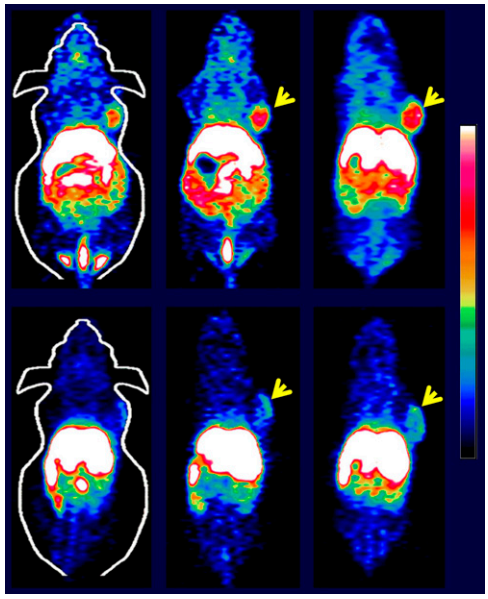

FIGURE 5. CD105-targeted imaging in a mouse model with a 4T1 tumor. Top row: Targeted, at (left to right) 4, 15, and 24 hours. Bottom row: Nontargeted, at (left to right) 4, 15, and 24 hours. PET imaging clearly demonstrated in vivo CD105 targeting of ^{64}Cu-CuS@MSN-TRC105. Highest tumor uptake was found to be ~6 %ID/g at 24 hours after injection. The nontargeted group showed $<$2 %ID/g tumor uptake.

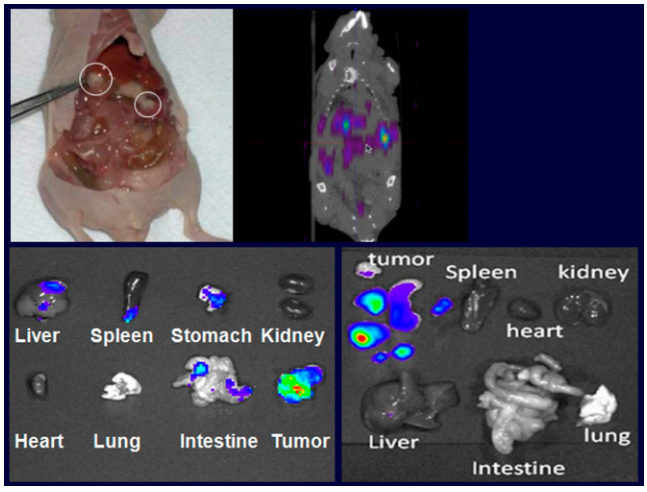

FIGURE 6. Top: Photographic and micro-SPECT/CT images of neutron-activated ^{166}Ho-mesoporous nanoparticles (MSNs) in mice bearing ovarian (SKOV-3) tumors. Bottom: Optical images of Cy5.5-labeled MSNs in mice bearing pancreatic (MIA PaCa-2) tumors at 24 hours (left) and 1 week (right).

cryosectioned tumor slices (Fig. 6). This could be a promising technique for delivering focal peritoneal therapy, for example, in ovarian cancer, as a form of brachytherapy. The authors noted that such an approach is expected to overcome limitations of radiation penetration, improve therapeutic responses, and reduce adverse events associated with "traditional" intraperitoneal brachytherapy.

Another area of current interest is in radiolabeling drugs. Petrulli et al. from Yale University (New Haven, CT) reported on "PET determination of specific uptake of ^{11}C-erlotinib by different tumor types expressing EGFR, in vivo through kinetic modeling" [544]. Erlotinib is a therapy for non–small cell lung cancer (NSCLC) and binds mutated but not wild-type EGFR. These researchers performed kinetic modeling and looked at binding potential. They found a high degree of intercellular mutated EGFR binding, but no significant binding with wild-type EGFR or in the absence of EGFR. They concluded that ^{11}C-erlotinib is a promising radiotracer that could become a clinical method for assessing EGFR–erlotinib interactions in patients with tumors that harbor EGFR-activating kinase domain mutations. This type of study points to our growing ability to predict which patients with specific tumor characteristics will respond to specific drug therapies.

Wehrenberg-Klee et al. from the Massachusetts General Hospital (Boston) reported on "Development of a HER3 PET probe for breast cancer imaging" [550]. HER3 is a receptor tyrosine kinase that forms heterodimers with HER2 and EGFR and that plays an important role in the pro-oncogenic signaling pathways of HER2-positive breast cancer. These authors developed an antibody-based PET probe (^{64}Cu-DOTA-HER3-F(ab)'2) specific for HER3, characterized it in vitro in a panel of HER3-expressing breast cancer cell lines, and performed in vivo PET/CT imaging in mouse xenografts (Fig. 7). They showed that HER3-

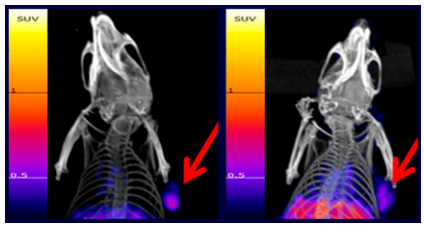

FIGURE 7. HER3-specific ^{64}Cu-DOTA-HER3-F(ab)'2 PET/CT imaging in (left) MDA-MB-468 and (right) HCC70 xenografts. Receptor cycling enables PET tumor visualization despite low HER3 expression, with xenografts imaged 24 hours after injection.

expressing breast tumors could be imaged using this novel probe and that standardized uptake values (SUV) correlated well with HER3 expression levels. Visualization was possible in xenografts even with very low levels of HER3 expression. The authors concluded that this probe might help guide the clinical development and use of HER3-targeted therapies.

Tripathi et al. from Thomas Jefferson University (Philadelphia, PA) reported on "Imaging bladder cancer: correlation with histopathologic findings" [67]. This group looked at vasoactive intestinal peptide receptor type 1 (VPAC1) as a regulatory receptor. The VPAC1 receptor is a member of the vasoactive intestinal polypeptide–pituitary adenylate cyclase-activating polypeptides that form a regulatory network in cell proliferation and transformation. VPAC1 receptors are overexpressed in high density on the cell membrane at the onset of oncogenesis of several cancers, including breast, prostate, and bladder cancers. The group previously cloned VPAC1 receptors and used a receptor-specific biomolecule (^{64}Cu-TP3805) for targeted PET imaging in breast and prostate cancer. A long-term goal across much of cancer care is to identify new strategies for distinguishing malignant lesions from benign masses and to thereby minimize unnecessary biopsies. These researchers showed high binding of their probe in breast cancer (Fig. 8) and prostate cancer. More recent work suggests that this agent can be useful in bladder cancer. When bladder cancer has metastasized, ^{18}F-FDG PET works quite well, but local disease may be more difficult to visualize because of

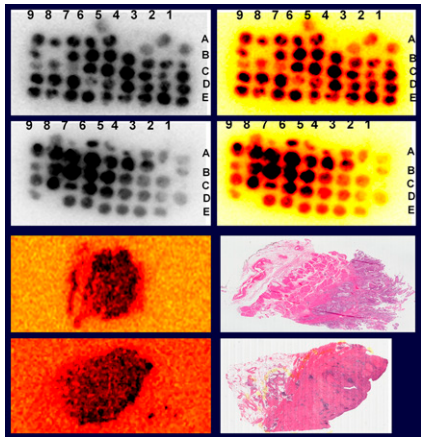

FIGURE 8. ^{64}Cu-TP3805 PET for VPAC1 targeting in bladder cancer. Top block: tissue microarray (n = 100; normal = 5). Bottom block: digital autoradiography with histology (n = 3)

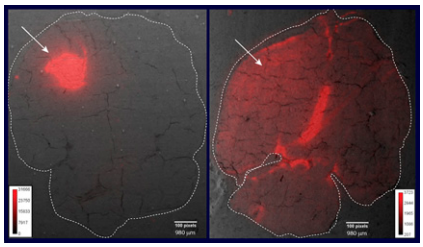

FIGURE 9. ^{225}Ac-DOTAGA-Substance imaging. ^{225}Ac-DOTAGA-Substance fluid was injected via the intracranial route in healthy mice brains, which were harvested at defined timepoints and sliced axially. Images are overlays of autoradiographic alpha camera system images and white light images at (left) 1 hour and (right) 4 hours after injection. Migration of the peptide from the original injected site (white arrow) is seen at 4 hours.

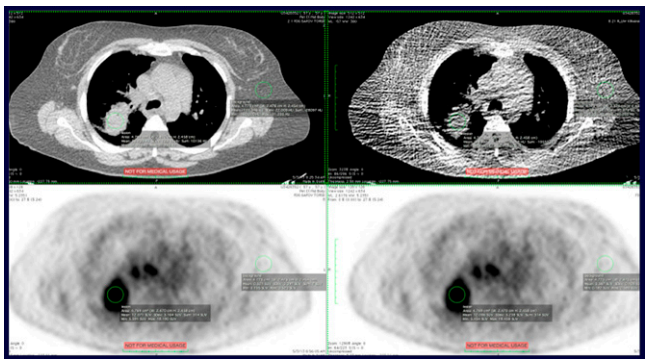

FIGURE 11. Attenuation correction with extreme CT dose reduction in whole-body FDG PET/CT. Top: CT with regular/clinical dose (left) and extreme dose reduction (right). Bottom: PET with clinically indicated CT dose (left) and CT extreme dose reduction (right). Low-dose CT acquisitions were acquired at 1/10 to 1/60th the dose of a clinical CT exam.

urinary excretion. ^{64}Cu-TP3805 is not excreted in urine, and so is promising as a PET agent for early bladder cancer.

We are seeing increasing research performed with α emitters, in part as a result of the recent success of ^{223}Ra-chloride. Abou et al. from Johns Hopkins University (Baltimore, MD), the Institute for Transuranium Elements (Karlsruhe, Germany), and the University of Gothenburg (Sweden) reported on "^{225}Ac imaging of NK1-targeted α-particle for glioblastoma radiotherapy" [393]. The researchers injected the tracer ^{225}Ac-Substance P into mouse brains and followed the distribution into the CSF space (Fig. 9). Most high-grade gliomas are highly vascular with a tendency to infiltrate, so it becomes quite difficult to deliver local therapy adequately and accurately. Because of tumor cycling and receptor expression, a higher dose is likely to be delivered locally to the glioblastoma. This research indicated that the NK1-targeted α-particles circulated and remained at target sites for up to 24 hours.

In addition to radiotherapy, photodynamic therapy is being explored. Photodynamic therapy causes free radical generation locally. Zhang et al. from the University of Pittsburgh (PA) reported on "Developing and evaluating therapeutic effect of a novel CB_2 receptor-targeted photosensitizer in cancer" [173]. Phototherapy allows for direct injury to locally irradiated tumor cells and tissues, but the technique is challenged by a lack of tumor sensitivity, so that normal tissues are damaged as well as tumor. These authors described type-2 cannabinoid receptor–targeted phototherapy using a novel photosensitizing agent, IR700DX-mbc94. They achieved good tumor growth delay in cutaneous models (Fig. 10). Such agents have potential for localized therapy in, for example, the esophagus, oropharynx, peritoneum, or other areas where light can be applied with relative ease.

Improving and Enhancing Information from Cancer Imaging

A number of papers at this meeting addressed ways in which we are improving the quality and types of information derived from images in humans. Christopfel et al. from the University of Washington (Seattle) and GE Global Research (Niskayuna, NY) reported on "Attenuation correction with extreme CT dose reduction for whole-body FDG PET/CT" [502]. Our community is involved in a widespread and ongoing effort to address the need to decrease radiation dose across the spectrum of medical imaging. These researchers acquired low-dose CT images at 1/10 to 1/60th of the doses of conventional clinical CT examinations. Although biasing and noise artifacts were apparent in the

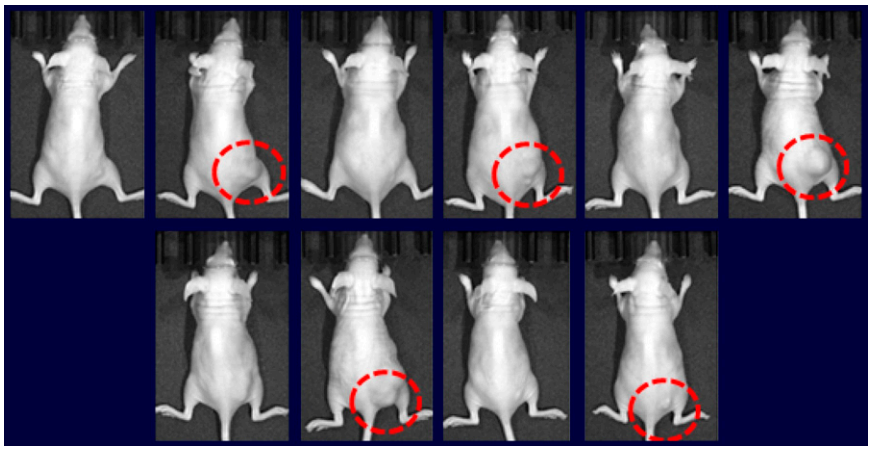

FIGURE 10. In vivo CB_2-targeted phototherapy. Top: Left image pair: Mice with no treatment at days 1 and 5; middle image pair: 1R700DX-mbc4 mice at days 1 and 5; right image pair: irradiation alone at days 1 and 5. Bottom: Left image pair: 1R700DX plus irradiation at days 1 and 5; right image pair: 1R700DX-mbc4 plus irradiation at days 1 and 5. The combination of IR700DX-mcb4 and irradiation results in the greatest tumor growth delay.

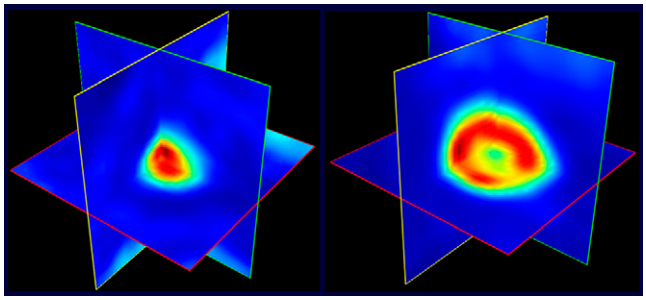

FIGURE 12. Entropy discriminates between (left) a nonnecrotic lesion (entropy = 2.03; SUV_{max} = 4.3; volume = 6.1 mL) and (right) a necrotic lesion (entropy = 2.9; SUV_{max} = 10.1; volume = 50 mL).

low-dose images, the visual appearance of the PET images was essentially the same when attenuation correction used either the regular or low-dose CT acquisitions (Fig. 11). In 4 patients, the maximum SUVs (SUV_{max}) of lung lesions did not change significantly from regular to low-dose CT attenuation correction, and background noise measured in uniform regions in the lung and abdomen were also largely unchanged between the 2 types of images. Despite the fact that image quality is less optimal in extreme dose reduction, the SUVs do not change significantly, suggesting that the low-dose acquisition can potentially be used routinely for attenuation correction.

One focus of increasing research aimed at deriving more information from images is in the exploration of intratumoral heterogeneity using texture indices. Orlhac et al. from IMNC-UMR (Orsay, France), Avicenne University Hospital (Bobigny, France), and CEA-Service Hospitalier Frédéric Joliot (Orsay, France) asked "Do texture indices derived from PET improve tumor characterization in NSCLC patients?" [453] In 48 patients with NSCLC, the researchers found that texture indices derived from ^{18}F-FDG PET showed promise in characterizing tumor histology (TN stage, level of differentiation, or necrosis) when ignoring other indices (i.e., in univariate analysis). When combined with SUV_{max} or tumor metabolic volume in multivariate analyses, textural indices provided no additional information (Fig. 12). They concluded that the informative value of textural indices should be investigated using multivariate analyses involving SUV_{max} and/or metabolic volume. The question for us is how can we best use these types of data and combine them to provide more value than the current available metrics.

Guo et al. from the Massachusetts General Hospital and Harvard Medical School (Boston) and National Taiwan University Hospital (Taipei) reported that "^{18}F-FLT PET/CT tumor heterogeneity is an effective biomarker in the diagnosis and staging of lung cancer" [123]. They performed intratumoral heterogeneity analyses for ^{18}F-FDG and ^{18}F-FLT, and their resulting data suggest that ^{18}F-FLT is better in differentiating among benign, early-, and advanced-stage disease. ^{18}F-FDG was unable to differentiate among these groups. They concluded that^{18}F-FLT tumor heterogeneity has great potential to augment diagnostic accuracy and improve tumor staging in oncologic practice. As the field moves forward, we will be better able to advance patient care by combining and analyzing some of these data we are already acquiring. The results should yield new kinds of prognostic information and help in avoiding unnecessary biopsies.

Zhang et al. from the Second Military Medical University and Changhai Hospital (Shanghai, China) and the Johns Hopkins University School of Medicine (Baltimore, MD) reported on "Using dynamic scanning and parametric imaging approach to improve quantification and visualization in oncology whole-body FDG PET-CT" [580]. These researchers used 1 minute per bed position and went through 5 or 6 bed positions, cycling through the whole body 10 or 11 times. They achieved spatial–temporal visualization of whole-body ^{18}F-FDG PET/CT and dynamic whole-body PET/CT quantification via parametric imaging. They quite nicely showed a Patlak plot image of the whole body and, in Figure 13, this is compared with the static image. They concluded that dynamic scanning with parametric imaging improved quantification and visualization of whole-body ^{18}F-FDG PET/CT and that parametric images and the spatial–temporal tracer uptake pattern have the potential to improve diagnostic accuracy and response monitoring of treatment. Using this technique, we could potentially produce whole-body Patlak plots and have available additional useful information about our ^{18}F-FDG datasets.

In addition to securing more information from the images we acquire, it is important to ensure that the interpretation process is more homogeneous. Marcus et al. from the Johns Hopkins Medical Institutions (Baltimore, MD) reported on "Head and neck PET/CT: therapy response interpretation criteria ('Hopkins criteria')" [344]. This group formulated scoring benchmarks for therapy assessment interpretation of head and neck ^{18}F-FDG PET/CT and investigated the accuracy, reader reliability, and predictive value for survival outcomes using these criteria in images in patients

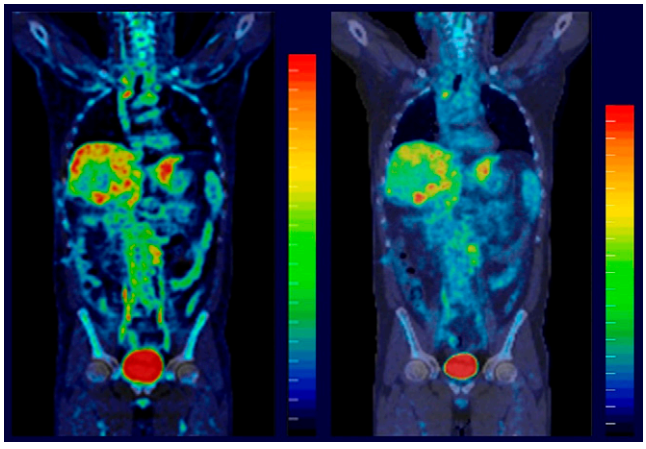

FIGURE 13. Quantification of dynamic whole-body ^{18}F-FDG PET/CT via parametric imaging. Left: K_i image by Patlak plot with spatial constraint (mL/min/100 mL). Right: clinical ^{18}F-FDG PET/CT 10-minute scan.

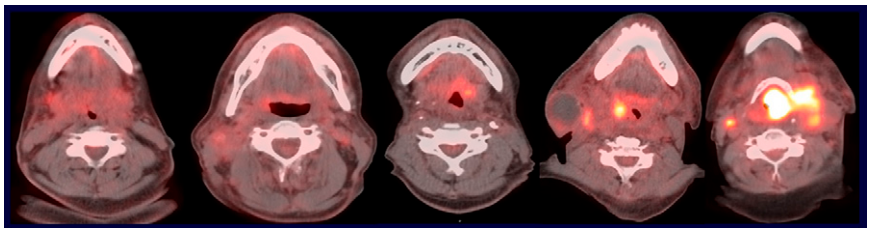

FIGURE 14. Developed Hopkins Criteria for interpretation of therapy response. Example images (left to right): score 1–FDG uptake at the primary site and nodes less than background blood pool (internal jugular vein, IJV); score 2–focal ^{18}F-FDG uptake at the primary site and nodes greater than blood pool (IJV) but less than liver; score 3–diffuse ^{18}F-FDG uptake at the primary site or nodes greater than blood pool (IJV) or liver; score 4–focal ^{18}F-FDG uptake at the primary site or nodes greater than liver; and score 5–focal and intense ^{18}F-FDG uptake at the primary site and nodes.

with head and neck squamous cell carcinoma (HNSCC). They found that specificity and negative predictive value were quite high with this scoring system. Especially in cases of low clinical suspicion for metastasis, the use of these criteria added value to PET/CT imaging. Use of the criteria predicted survival outcomes in HNSCC patients with residual disease at a single site after therapy and also predicted survival outcomes in human papilloma virus–positive HNSCC patients after therapy (Fig. 14). Again, this is one of the methods by which we are not only improving imaging but identifying new ways to improve interpretation of these images.

Another area of continuing interest is in nuclear and intraoperative optical imaging for lymph node dissections. Van den Berg et al. from Leiden University Medical Center (The Netherlands), Eurorad (Strasbourg, France), and NKI-AvL (Amsterdam, The Netherlands) reported on "Evaluation of an opto-nuclear probe for combine radio- and fluorescence-guided sentinel node biopsy" [59]. The prototype opto-nuclear probe is a modified gamma probe with built-in optical fibers allowing acoustic gamma tracing and acoustic fluorescence tracing. They evaluated the use of the device in detection of the hybrid tracer indocyanine green–^{99m}Tc-nanocolloid in ex vivo studies. The probe accurately predicted the presence/absence of radioactivity in 100% of excised sentinel nodes. Fluorescence tracing was correct in 72% of these nodes. By tailoring the photomultiplier tube for fluorescence detection the sensitivity increased to 97%. The intention is to translate this to in vivo studies. Again, we are developing not only new multimodality imaging tracers but also multimodality probes for acquiring imaging information.

Hypoxia remains a focus of great interest in both diagnosis and therapy. Verwer et al. from VU University Medical Center (Amsterdam, The Netherlands), and Maastricht University Medical Center (The Netherlands) reported on "Quantification of hypoxia in NSCLC patients using [^{18}F]HX4" [9]. This agent is somewhat more hydrophilic than traditional hypoxia imaging agents such as ^{18}F-MISO. The group reported on the development of a kinetic model for quantifying uptake of ^{18}F-HX4. Results suggested that reversible 2-tissue compartment pharmacokinetic modeling was best in their study population of NSCLC patients. What is useful about having the appropriate model, of course, is that accurate data is available about hypoxia to inform therapy guidance, radiotherapy boost, and prognosis. Figure 15 shows imaging at different time periods using the developed model.

The other key aspect related to hypoxia is perfusion: when less blood is available, less oxygen is present. Fletcher et al. from Indiana University School of Medicine (Indianapolis) reported on "Whole-body PET/CT evaluation of tumor perfusion using generator-based ^{62}Cu-ETS: Validation by direct comparison to ^{15}O-water" [446]. The "microsphere-like" tracer ^{62}Cu-ETS (ethylglyoxal bis(thiosemicarbazon)copper(II) provided k_1 bloodflow values in milliliters per minute per gram of tissue that were highly correlated with reference standard ^{15}O-water. This correlation was found in 3 normal tissues (muscle, myocardium, and thyroid) as well as metastatic lesions on PET/CT. Figure 16 shows examples from before and during therapy, in which whole-body PET/CT images were obtained with the ^{62}Cu-ETS radiopharmaceutical. The authors pointed to the potential for this agent in patients with metastatic renal cancer. SUV as a means for determining additional information about tissue/tumor blood flow can enhance available imaging data about antiangiogenic therapies.

Theranostics—the combination of therapeutic and diagnostic agents—is an area of growing interest in nuclear medicine. At this meeting, Giraudet et al. from the Léon Bérard Cancer Institute (Lyon, France) reported on "SYNFRIZZ–a phase Ia/Ib of a radiolabeled monoclonal AB for the treatment of relapsing synovial sarcoma" [223]. This group is working with a monoclonal antibody radiolabeled with indium for targeting and yttrium for therapy. Figure 17

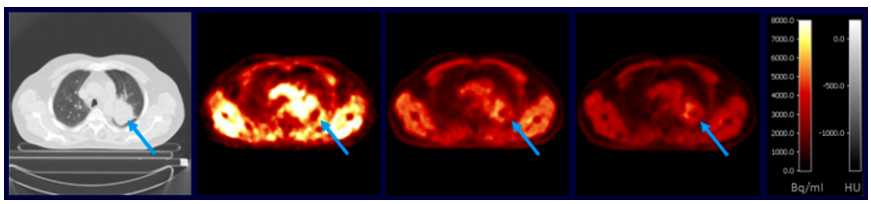

FIGURE 15. ^{18}F-HX4 quantification of hypoxia in non–small cell lung cancer. Left to right: low-dose CT; ^{18}F-HX4 PET acquired 25–30 minutes after injection; ^{18}F-HX4 PET acquired 240–270 minutes after injection.

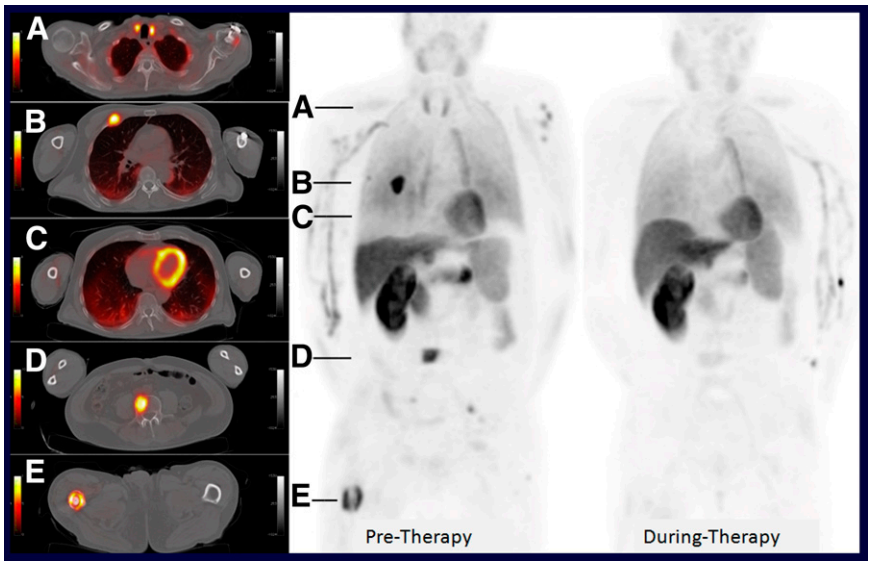

FIGURE 16. ^{62}Cu-ETS hypoxia perfusion imaging acquired in a patient with metastatic renal cell cancer. Left column: transaxial slices through torso before therapy. Middle: pretherapy torso scan with corresponding sites of high ^{62}Cu-ETS uptake in (A) normal thyroid, (B) anterior right rib bone metastases, (C) normal myocardium, (D) lumbar spine metastases, and (E) right femoral bone metastases. Right: Torso image during therapy reflects decrease in tumor bloodflow during 4-week therapy with sunitinib.

shows initial data on metastatic synovial sarcoma screening with ^{111}In-OTSA, which targets the FZD-10 antigen overexpressed in synovial sarcomas. Uptake on imaging was graded. They reasoned that higher grade tumors or tumors with more of the epitope expressed were more likely to respond to therapy. They randomized patients more likely to respond to therapy to low- or high-dose (370 and 1,110 MBq, respectively) ^{90}Y-OTSA therapy. I believe that these types of theranostic combinations will continue to grow in numbers and applications, especially as the number of targeted epitopes expands. The advantages are not only in the development of new therapy but in accurately identifying patients who are most likely to respond to specific therapies.

Kulkarni et al. from the Zentralklinik Bad Berka (Germany) reported on "Efficacy of single- or duo-radionuclide peptide receptor radionuclide therapy (PRRT) in 1,000 patients with neuroendocrine neoplasms (NENs): analysis from a single center over more than 10 years" [396]. This is perhaps the largest cohort of patients in whom dual-agent imaging and therapy have been studied. This retrospective analysis was performed in individuals with metastatic and/or progressive NENs, undergoing 1–9 cycles of PRRT using ^{177}Lu (n = 331), ^{90}Y (n = 170), or both (n = 499). Patients were followed for up to 132 months after the first cycle of PRRT. The authors concluded that PRRT lends a significant benefit in overall survival in metastasized and/or progressive G1–2 neuroendocrine tumors when compared with other treatments and regardless of previous therapy. The combination of ^{177}Lu and ^{90}Y for PRRT may be more effective than either radionuclide alone, with results especially evident in earlier disease (Fig. 18). Many of these patients had undergone therapy previously, suggesting that they had fewer treatment options.

As noted previously, another therapy drawing much current research and clinical interest is ^{223}Ra for bone metastasis in prostate cancer. Conti et al. from the University of Southern California (Los Angeles), the Washington University School of Medicine (St. Louis, MO), Algeta ASA (Bayer) (Oslo, Norway), Bayer HealthCare (Whippany, NJ), and Karolinska University Hospital (Stockholm, Sweden) reported on "Radium-223 dichloride (radium-223) hematologic and 1.5-year posttreatment safety in patients with castration-resistant prostate cancer (CRPC) and symptomatic bone metastases: From ALSYMPCA" [208]. One question about this new therapy is whether ^{223}Ra administration is associated with sequelae of any type. Monitoring of patients who receive ^{223}Ra is essential in building a complete safety profile. In such monitoring, these authors found very low hematologic adverse event rates. During treatment anemia rates were relatively low, with slightly more neutropenia

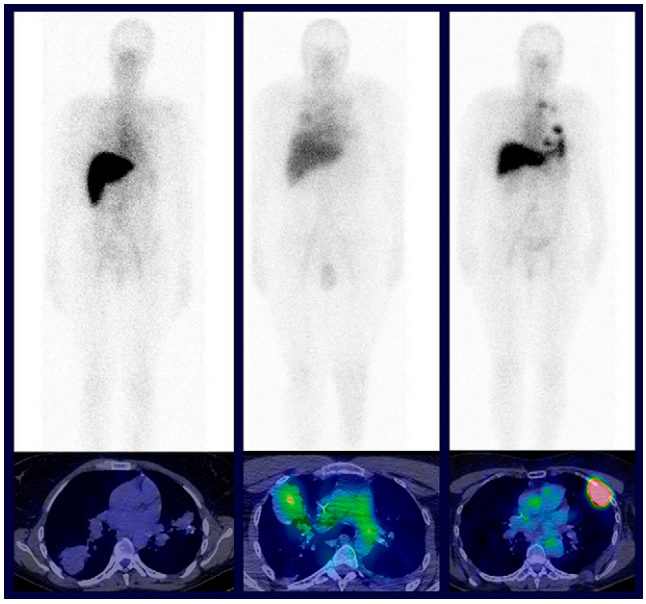

FIGURE 17. Examples of ^{111}In-OTSA visual assessment in metastatic synovial sarcoma, with assigned grades of (left to right) grade 1 (uptake < mediastinum), grade 3 (uptake > mediastinum < liver, grade 4 (uptake = ≥ liver).

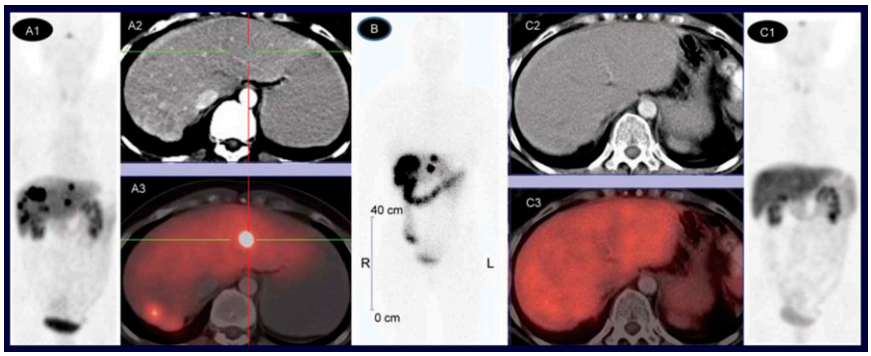

FIGURE 18. Peptide receptor radionuclide therapy (PRRT) in neuroendocrine neoplasms. ^{68}Ga-DOTATOC images pretherapy (panels A, B) show multiple foci of disease pretreatment. Images posttreatment (panel C) show complete remission of disease after dual ^{177}Lu and ^{90}Y PRRT.

and thrombocytopenia than comparative placebo groups. A total of 571 patients entered long-term follow-up, and, at 1.5 years, the ^{223}Ra and placebo groups showed similar rates of all grade 3/4 hematologic adverse (19% and16%, respectively), neutropenia (2% and 1%, respectively), thrombocytopenia (6% and 2%, respectively), and anemia (13% and 13%). Only 1 case of febrile neutropenia was seen during treatment, and only 1 case of aplastic anemia was seen during long-term follow-up (in a patient who had been previously treated with docetaxel and another radionuclide). No safety concerns were noted. This therapy thus has the potential to be combined with other nonradioactive therapies in studies designed to prolong survival in patients with prostate cancer.

Combined modalities were again a focus at this meeting, including PET/MR. Head and neck cancer is an area that lends itself to PET/MR, in part because of the low image quality often achieved in this area with CT. Purz et al. from University Hospital Leipzig (Germany) reported on "Correlation of multimodal functional parameters of simultaneous ^{18}F-FDG PET/MRI in patients with head and neck cancer" [289] (Fig. 19). The researchers used the dual modality to simultaneously cross-evaluate glucose metabolism, cellularity, and vascularization in patients with head and neck cancer (Fig. 20). The researchers found significant correlation between SUV_{mean} and K^{trans} and between SUV_{mean} and k_{ep}. The data yielded information about both metabolism and perfusion, providing complementary data about 2 different aspects of the disease. Much work remains to be done, not only in head and neck cancer but in other cancers, to explore the additional value that can result from combining different parameters from different modalities as opposed to looking at their individual results alone.

From First-in-Human to Multicenter Trials

Wester et al. from the Technische Universität München (Garching and Munich, Germany) reported on "Imaging of CXCR4 chemokine receptor expression with [^{68}Ga]Pentaxifor: First experience in cancer patients" [118]. Pentixafor is a cyclic pentapeptide with high affinity and selectivity to hCXCR4. The authors reported first experiences with this agent using PET/CT and PET/MR imaging in patients with various cancers. Intense tracer uptake was seen in chronic lymphocytic leukemia and lymphoma as well as a range of epithelial cancers. It will be interesting to see how this and other tracers aimed at receptor expression and targeted therapy develop over time.

Interesting work is also being done in hepatocellular carcinoma (HCC), where ^{18}F-FDG may not be the optimal PET agent. Castilla-Lièvre et al. from APHP Hôpital Antoine Béclère (Clamart, France) and Service Hospitalier Frédéric Joliot–CEA (Orsay, France) reported on "A prospective evaluation of dual tracers ^{11}C-choline and ^{18}F-FDG PET-CT in HCC" [572], looking at glucose metabolism and lipid metabolism to determine whether the additional information was revealing. The study included 33 patients with suspicious HCC in cirrhotic liver who underwent PET/CT with both ^{11}C-choline and ^{18}F-FDG. The authors found that not all patients who showed ^{11}C-choline uptake showed ^{18}F-FDG uptake, and vice versa. PET/CT with the 2 tracers proved to be not only an excellent diagnostic marker of HCC with overall sensitivity of 96% but also a significant prognostic marker. More agressive HCC was more often detected by ^{18}F-FDG, whereas hypermetabolic ^{11}C-choline lesions were more frequently associated with a better prognosis. They concluded that this combined tracer approach should be routinely used in the diagnosis of HCCs in cirrhotic livers and for a better selection of patients for surgical resection or liver transplantation. In carcinoid tumors as well we sometimes see that as levels of cell surface receptors go down, ^{18}F-FDG uptake goes up. I believe that these and other tumors change over time, so that looking at

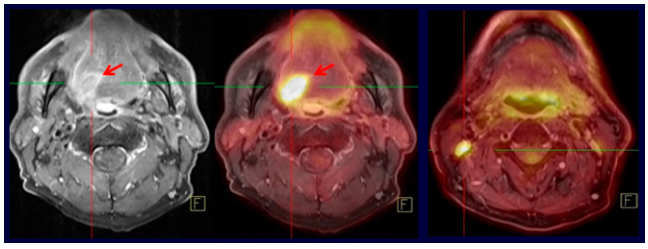

FIGURE 19. ^{18}F-FDG PET/MR in a patient with head and neck cancer. Left to right: MR demonstrating tongue-based lesion, ^{18}F-FDG PET/MR fusion shows increased glucose metabolism in the lesion, fusion image at an additional level shows metabolic activity in a lymph node metastasis.

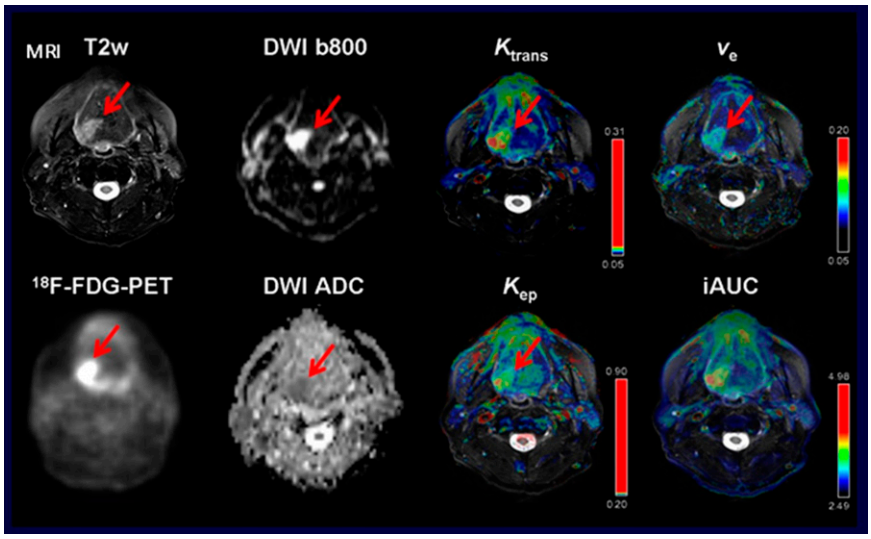

FIGURE 20. ^{18}F-FDG PET/MR of a patient with head and neck cancer. Top row (left to right): T2-weighted MR; diffusion-weighted MR; transfer constant (k_{trans}) MR map; interstitial volume (v_e) MR map. Bottom row (left to right): ^{18}F-FDG PET; diffusion-weighted apparent diffusion coefficient MR; rate constant (k_{ep}) MR map; initial area under the uptake curve (iAUC) contrast-enhanced MR.

more than one tracer may prove useful in understanding the temporal evolution of tumor dedifferentiation across metastatic foci. Figure 21 from this study shows a hypermetabolic lesion with ^{18}F-FDG and hyper- and hypometabolic lesions with ^{11}C-choline.

Hartenbach et al. from the German Federal Armed Forces Hospital (Ulm), Ludwig Maximilians University (Munich, Germany), and Medical University Vienna (Austria) reported on "Therapy monitoring of advanced HCC using ^{18}F-ethylcholine-PET/CT" [575]. These researchers looked at SUV_{mean}, SUV_{max}, change in SUV_{max}, and at tumor-to-spleen ratio in patients with locally advanced disease. Combining these data yielded a very high area under the curve of 0.9 as a marker for response to selective internal radiation therapy. This is another example of research being done with new tracers to maximize the amount of useful information gleaned from a given imaging dataset. Larger studies are likely to provide additional insights on the contributions of new tracers and analytical methods to maximize information that can be derived from their use.

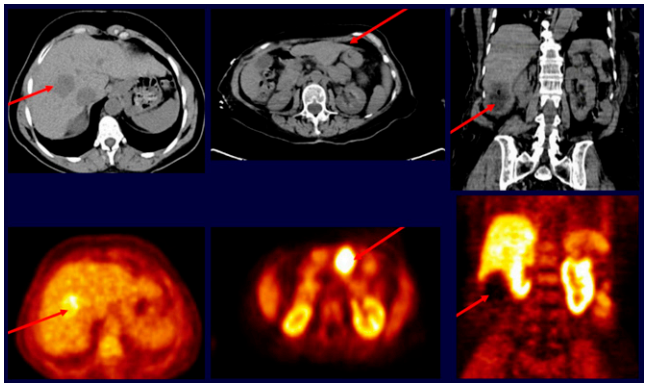

FIGURE 21. ^{11}C-choline and ^{18}F-FDG PET/CT in hepatocellular carcinoma. Left: hypermetabolic lesion on ^{18}F-FDG. Middle: hypermetabolic lesion on ^{11}C-choline PET/CT. Right: hypometabolic lesion on ^{11}C-choline PET/CT.

Vigil et al. from the Clinica Universidad Navarra (Pamplona, Spain) reported on "Prediction of recurrence and survival analysis after radiotherapy of glioblastoma using ^{11}C-methionine PET/CT and MR" [12]. These authors studied the relationship between the distribution ^{11}C-methionine on PET/CT prior to radiation therapy for glioblastoma and location of subsequent recurrence, with additional evaluation of association with survival and location of recurrence. They found that gross tumor volumes were increased by an average of 3 cc when ^{11}C-methionine PET/CT was added to MR tumor volume data. In 33 of 46 patients (75%) the recurrence location on MR imaging matched the highest methionine uptake areas on PET/CT (Fig. 22). Higher ^{11}C-methionine correlated with lower

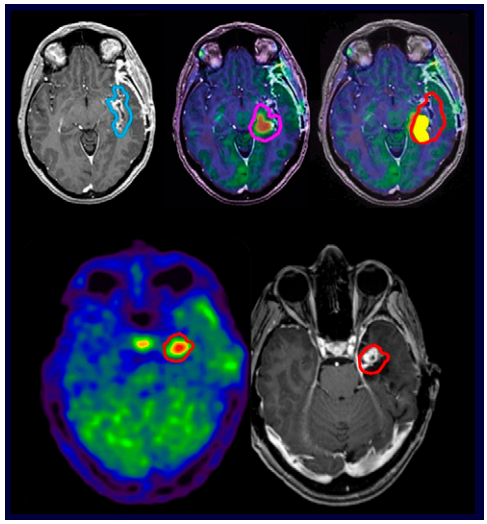

FIGURE 22. ^{11}C-methionine PET/CT and MR in glioblastoma. Top: Gross tumor volume (GTV) on MR (left) and ^{11}C-methionine PET/CT (middle) yielded a median 3.12 cc of volume (range, 0.84–0.848) not identified on MR imaging alone. Bottom: Recurrence volume on MR imaging (right) matched areas of highest uptake on ^{11}C-methionine PET/CT (left) in 33 of 46 patients.

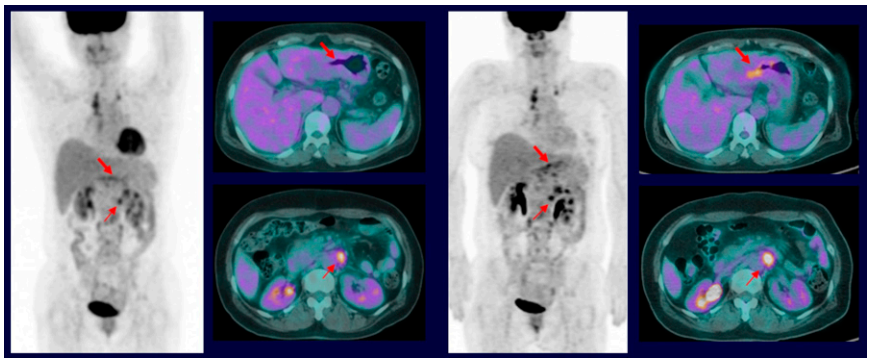

FIGURE 23. PPAR-γ agonist administration and ^{18}F-FDG PET imaging in a 53-year-old woman with signet ring cell gastric carcinoma and multiple lymph node metastases. Left block: Images acquired 1 day before pioglitazone administration. Right block: images acquired 2 days after pioglitazone demonstrate an increase in SUV_{max} with agonist administration.

overall and progression-free survival, leading the authors to conclude that uptake patterns on ^{11}C-methionine PET/CT have a role in predicting relapse as well as a prognostic value and could become a useful adjunct for optimal treatment planning. This is one of a number of studies suggesting the potential added value of hybrid and/or coregistered multimodality imaging.

We continue to look for ways to better distinguish tumor from inflammation and to accurately target therapeutic agents in settings where inflammation and tumor coexist. Han et al. from Chonbuk National University Medical School and Hospital (Jeonju, Republic of Korea) reported on "Phase II clinical trial to validate usefulness of pioglitazone to differentiate cancerous from inflammatory lesions in patients undergoing FDG PET/CT" [230]. These researchers had previously shown in a preclinical study that ^{18}F-FDG uptake was enhanced in tumors and decreased in benign lesions after administration of a peroxisome proliferator-activated receptor (PPAR-γ) agonist. They reported on a current study designed to use such an agent to aid in differentiating tumor from inflammation in a clinical trial. They found that ^{18}F-FDG SUVs were increased in tumors relative to inflammation in patients after administration of the agonist. Figure 23 is an example from a gastric cancer, where the SUV increased by 76% after PPAR-γ agonist administration. This is somewhat analogous to techniques such as fasting patients to increase tumor-to-background ratio. Similar therapeutic interventions that allow us to identify and target disease more effectively are under current development.

Cope et al. from Navidea Biopharmaceuticals (Dublin, OH) and The Ohio State University (Columbus, OH) reported that "The CD206-targeted, macrophage (MP)-localizing ^{99m}Tc-tilmanocept is accrued ~3-times greater in tumor-positive sentinel lymph nodes (SLNs) than tumor-negative SLN and 18-times greater than non-SLNs" [285]. They concluded that targeting CD206 with ^{99m}Tc-tilmanocept results in significant discrimination of SLNs with tumor from those without tumor. One notable point is that 39 patients with persistent nodal HNSCC disease (47% of the intent-to-treat population) were included in the interim analysis, with only one false-negative, yielding a false-negative rate of only 2.56%. This type of agent might also be useful for looking at tumor-associated macrophages, which can carry a great deal of prognostic information in terms of the ways in which tumors will respond to therapy. This kind of research also points toward the potential for using the same type of agent not only for lymph node imaging but for therapy guidance at primary or metastatic sites.

Minamimoto et al. from Stanford University (CA), University of Nebraska (Omaha), MD Anderson Cancer Center (Houston, TX), and RWTH Aachen University (Germany) reported on a "Multicenter study for comparison of FLT and FDG PET/CT for early interim therapy monitoring of diffuse large B-cell lymphoma" [594].

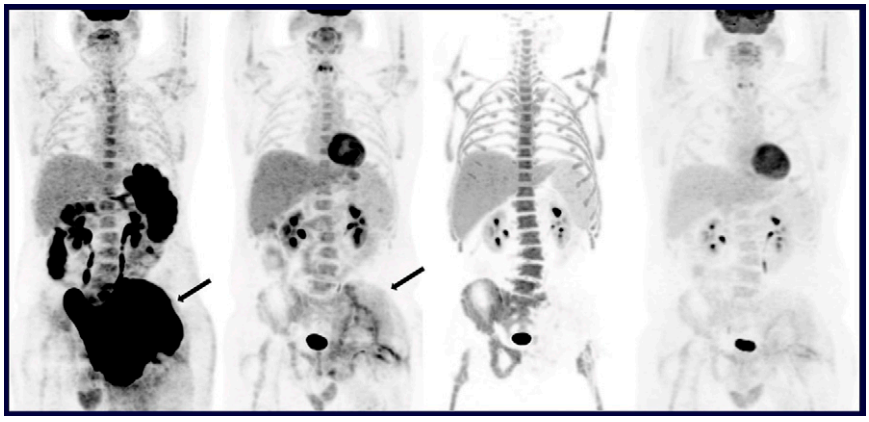

FIGURE 24. ^{18}F-FDG and ^{18}F-FLT PET in diffuse large B-cell lymphoma. Example images in a patient before and after R-CHOP therapy (left to right): ^{18}F-FDG PET at baseline; ^{18}F-FDG PET after 2 cycles of therapy indicating a partial response; negative ^{18}F-FLT after 2 cycles of therapy; and end-of-treatment ^{18}F-FDG PET indicating complete response.

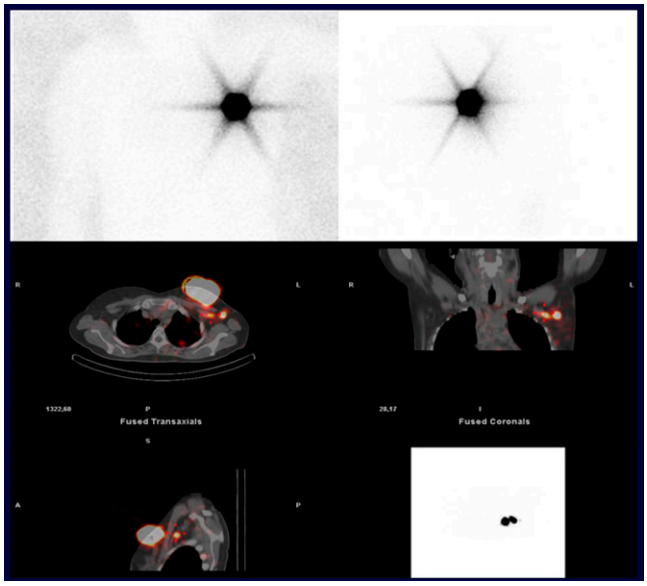

FIGURE 25. Planar imaging versus SPECT/CT sentinel lymph node imaging in a 49-year-old woman with a tumor (T2N0M0) in the upper inner quadrant of the left breast. Top: no sentinel lymph node (SLN) is visible on planar anterior and left lateral images. Bottom: Two axillary SLNs are visible on SPECT/CT directly behind the tumor, demonstrating the utility of SPECT/CT over planar imaging for this assessment.

^{18}F-FDG is currently widely used for interim therapy monitoring in lymphomas, and these researchers wanted to assess the comparative value of ^{18}F-FLT in predicting response after R-CHOP therapy for diffuse large B-cell lymphoma. Negative predictive values for complete response were quite high using standard ^{18}F-FDG criteria as well as ^{18}F-FLT (both 100%) in this 21-patient group. However, interim ^{18}F-FLT PET/CT showed significantly higher positive predictive values than ^{18}F-FDG PET/CT for interim (post-cycle 2 R-CHOP) response assessment. Figure 24 presents examples from this study. Residual

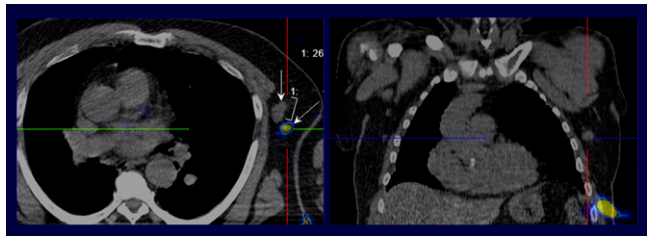

FIGURE 27. SPECT/CT in sentinel lymph node imaging in a patient with melanoma of the left thorax. Fusion SPECT/CT images show a single axillary sentinel lymph node (SLN). An additional "cold" lymph node was identified on the CT images near the SLN. Histologic results were positive for metastatic involvement, highlighting the utility of multi-modality imaging.

tracer uptake is confounding in many similar treatment monitoring studies, resulting in false-positives. In this case ^{18}F-FLT appears to be a potentially useful alternative to ^{18}F-FDG.

Two trials from the International Atomic Energy Agency (IAEA) compared SPECT/CT and planar imaging in SLNs. Jiménez-Heffernan et al. from the Hospital Juan Ramón Jiménez Huelva, Spain), Stellenbosch University and Tygerberg Hospital (Tygerberg, South Africa), University of Sao Paolo (Brazil), Manipal Hospital (Bangalore, India), Fundación Arturo López Pérez (Santiago, Chile), Centre Hospitalier Lyon (France), Universidade Federal de Pernambuco (Recife, Brazil), University of Santo Tomas (Manila, Philippines), The Netherlands Cancer Institute (Amsterdam), and the IAEA (Vienna, Austria) reported on "Prospective IAEA sentinel node trial on the value of SPECT/CT vs planar imaging in various malignancies" [565]. This group looked at patients with breast cancer (n = 1,182), melanoma (n = 262), and pelvic cancer (n = 64) from 16 centers in 11 countries. Significantly more sentinel nodes were detected by SPECT/CT than planar imaging. In pelvic cancers they found a 50% drainage basin mismatch

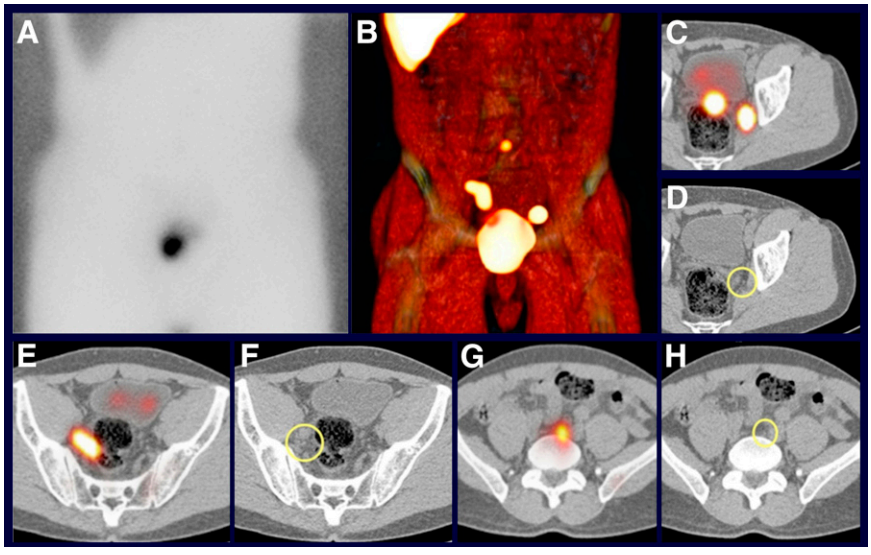

FIGURE 26. Planar imaging versus SPECT/CT sentinel lymph node imaging in a patient with prostate cancer with no evident lymphatic drainage on anterior planar imaging (A) SPECT/CT displayed with volume rendering (B) shows drainage to obturator lymph nodes in both sides of the pelvis and to a subaortic lymph node. These sentinel nodes, seen as hot spots on transverse SPECT/CT fusion images (C, E, and G), correspond with normal-sized lymph nodes (circles) on CT (D, F, H). Note that the right obturator hot spot is elongated and corresponds with a cluster of lymph nodes.

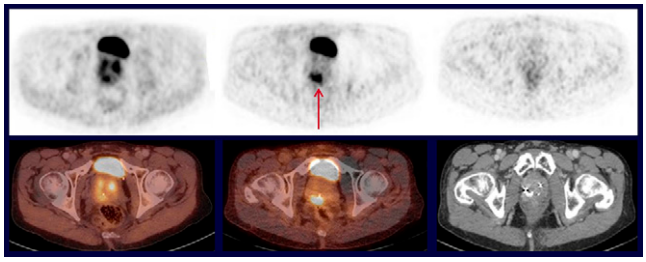

FIGURE 28. GRPR antagonist ^{68}Ga-RM2 PET and prostate cancer. PET (top row) and PET/CT (bottom row) in a 64-year-old man with primary prostate carcinoma and benign prostatic hyperplasia (BPH) and tumor positive biopsies with Gleason scores of 7a. The patient underwent external beam radiation therapy of the prostate with 54 Gy plus dose escalation to 74 Gy of the ^{68}Ga-RM2 PET–positive area. Left: ^{18}F-FECH images acquired at first examination before therapy did not distinguish between tumor and BPH; middle: ^{68}Ga-RM2 acquired at first examination before therapy shows focal tumor; right: ^{68}Ga-RM2 images acquired at second examination after irradiation, with no tumor visible.

with the 2 imaging techniques, resulting in surgical adjustment in 64% of cases, strongly suggesting that SPECT/CT is preferable over planar imaging in many of these cases. In Figure 25 SLNs in a patient with breast cancer are hidden because of overlap with the tumor on the AP view; with SPECT/CT, these are visible. In Figure 26, nodes that might be missed on planar imaging are visible on SPECT/CT, which has the advantage of providing additional information valuable for surgical planning.

Another group using data from the same large IAEA trial looked at SPECT/CT and planar imaging specifically in melanomas. Huic et al. from University Hospital Centre Rebro Zagreb (Croatia), Real Hospital Portugues de Beneficencia em Pernambuco (Recife, Brazil), Universidade de São Paulo (Brazil), Fundación Arturo López Pérez (Santiago, Chile), University Hospital Alexandrovska Medical University (Sofia, Bulgaria), Pretoria Academic Hospital (South Africa), Instituto Nacional de Cancerología (Bogotá, Colombia),

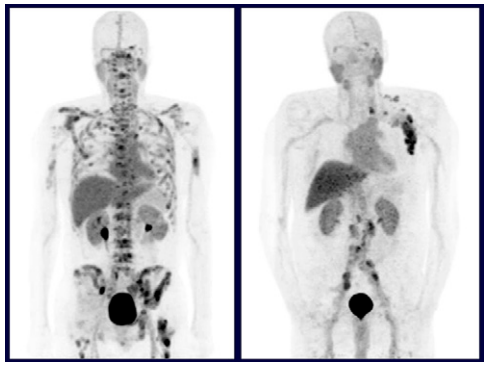

FIGURE 29. PSMA-targeting ^{18}F-DCFBC PET images demonstrating (left) widespread bone metastases in a patient with castration-resistant prostate cancer and (right) nodal metastases (supraclavicular, axillary, retroperitoneal) in a patient with castration-sensitive prostate cancer.

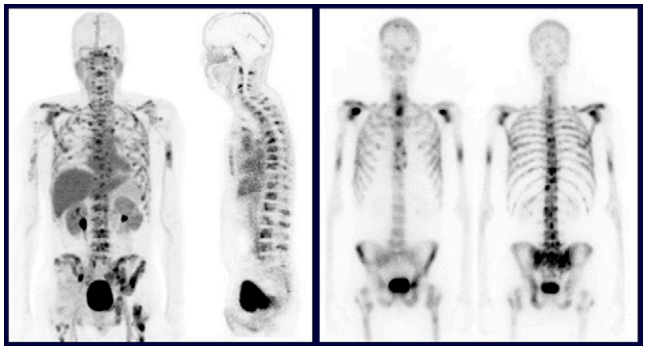

FIGURE 30. Widely disseminated bone metastases in a patient with prostate cancer imaged with (left pair) ^{18}F-DCFBC PET and (right pair) ^{99m}Tc-MDP bone scintigraphy, demonstrating numerous additional lesions identified using PSMA-targeted imaging.

Sofia Cancer Center (Bulgaria), University of Santo Tomas (Manila, Philippines), and the IAEA (Vienna, Austria) reported on "The added value of SPECT/CT in sentinel node identification in melanoma patients—a prospective multicenter IAEA study" [654]. They identified a positive impact of SPECT/CT findings on surgeons' decision making in ~50% of the study's 262 patients, helping to guide therapy and improve results. In example images in a melanoma of the left thorax (Fig. 27), 2 lymph nodes are visible. The large node has no uptake on SPECT, whereas the smaller one shows uptake; combining information from both modalities helps provide the needed information to more accurately guide therapy.

Prostate Imaging

We have many different ways to image prostate cancer and a growing number of agents and targets. It may take a few years to sort out which are most useful in specific applications, but no one agent is likely to answer every question in every instance. At this meeting we heard from several groups who are exploring new agents. Wieser et al. from the University Hospital Freiburg (Germany) and Piramal Imaging GmbH (Berlin, Germany) reported on "Gastrin-releasing peptide receptor (GRPR) antagonist

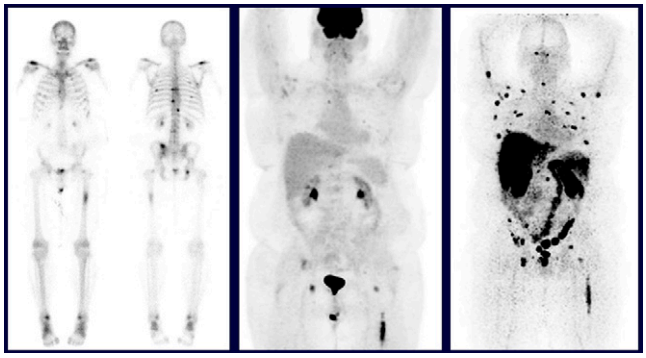

FIGURE 31. ^{89}Zr-IAb2M minibody imaging. Images acquired in a man with metastatic prostate cancer and rising prostate-specific antigen with: (left) ^{99m}Tc bone scanning; (middle) ^{18}F-FDG PET; (right) ^{89}Zr-Df-IAB2M anti-PSMA minibody imaging.

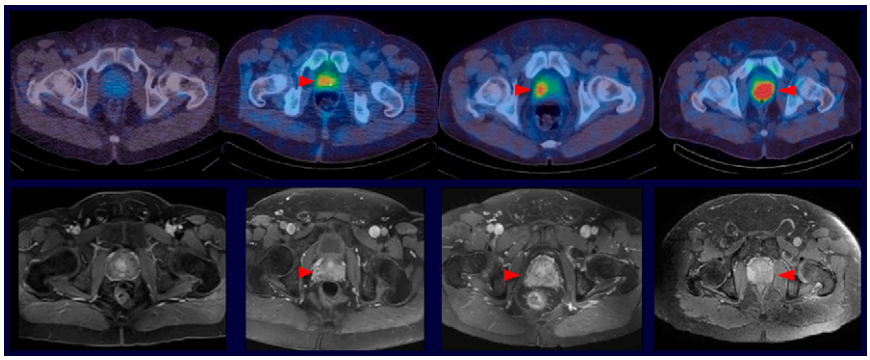

FIGURE 32. Examples of fused axial ^{99m}Tc-trofolastat SPECT/CT reconstructions (top row) and matching axial contrast-enhanced MR images (bottom row) in (left to right): healthy volunteer (PSA = 1.6 ng/mL); patient with Gleason score of 3+4 (PSA = 19.2 ng/mL); patient with Gleason score of 4+3 (PSA = 6.6 ng/mL); and patient with Gleason score of 4+5 (PSA = 61.3 ng/mL). Red arrowheads indicate location of histologically confirmed primary prostate lesions.

^{68}Ga-RM2 as PET tracer for imaging prostate cancer: Initial experiences" [17]. The study included 24 patients with prostate cancer (9 primary tumors, 15 recurrence) who underwent ^{68}Ga-RM2 PET imaging. In primary tumors in 8 of 9 (89%) patients ^{68}Ga-RM2 PET provided lesion delineation. One primary tumor (Gleason 9) showed no detectable GRPR expression. In 14 of 15 patients, previous standard imaging provided negative or inconclusive results for recurrence. However, ^{68}Ga-RM2 PET depicted GRPR-positive recurrences and/or metastases in 7 of these 15 patients (47%). In the remaining 8, no tumor manifestation could be detected by ^{68}Ga-RM2 PET or subsequent imaging studies. Figure 28 shows a patient with primary prostate cancer. ^{18}F-FECH PET is equivocal with both tumor and BPH tracer uptake, whereas the tumor is differentiated from BPH on ^{68}Ga-RM2 PET, with signal disappearing on ^{68}Ga-RM2 PET after radiotherapy. However, it is important to remember that no one agent will be better in every instance. We will find, for example, that not all prostate tumors have prostate-specific membrane antigen (PSMA) overexpression, that some prostate tumors will not have amino acid transporter upregulation and some will have no fatty acid utilization upregulation. Overall, however, I believe that many of the agents in development across these distinct imaging target classes will work much better than our current standard of care techniques.

Rowe et al. from Johns Hopkins University (Baltimore, MD) reported on "[^{18}F]DCFBC (DCFBC) prostate-specific membrane antigen (PSMA) based PET/CT detection of metastatic castration-sensitive and castration-resistant prostate cancer" [19]. The study with this low-molecular-weight PSMA agent was performed in 12 patients with rising PSA and radiographic evidence of metastatic prostate cancer by CT and/or bone scan. Figure 29 shows that ^{18}F-DCFBC PET/CT identified bone metastases as well as nodal metastases. In Figure 30, ^{18}F-DCFBC PET imaging revealed many more osseous lesions than a corresponding ^{99m}Tc-MDP planar bone scan. ^{99m}Tc-MDP is a relatively insensitive marker for bone metastases compared to some of these newer agents in development.

Pandit-Taskar et al. from the Memorial Sloan–Kettering Cancer Center (New York, NY) and ImaginAb, Inc. (Inglewood, CA) reported on "^{89}Zr-IAb2M minibody imaging in patients with prostate cancer: biodistribution, kinetics, lesion uptake, and organ dosimetry" [1670]. The phase I trial was conducted in 11 patients with metastatic prostate cancer using this radiolabeled agent targeting PSMA. In the patient in Figure 31, the ^{99m}Tc bone scan indicates few lesions and the ^{18}F-FDG scan is fairly insensitive, but ^{89}Zr-Df-IAB2M anti-PSMA minibody imaging shows numerous metastatic sites. PSMA is clearly a good target, and we as a field are developing multiple ways of looking at it.

Goffin et al. from University Hospitals Leuven (Belgium), Jahn Ferenc South Pest Hospital (Budapest, Hungary), Vanguard Urology (Houston, TX), University of Washington (Seattle), Weill Cornell Medical College (New York, NY), and Progenics Pharmaceuticals (Tarrytown, NY) reported on "A phase 2 study of ^{99m}Tc-trofolastat (MIP-1404) to identify prostate cancer in high-risk patients undergoing radical prostatectomy and extended pelvic lymph node dissection: an interim analysis" [15]. These researchers found that their PSMA-targeting agent correlated quite well with lesion score and had much better sensitivity than MR imaging, localizing more accurately to disease sites. Figure 32 shows example scans, with higher Gleason scores correlating with more uptake of PSMA-targeted agent. The authors concluded that this agent may be particularly useful in providing additional information about disease aggressiveness in high-risk patients prior to surgery.

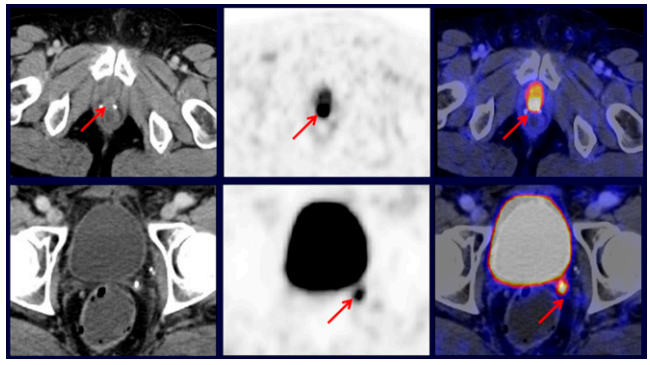

FIGURE 33. Examples of local prostate cancer recurrence imaged by ^{68}Ga-PSMA PET/CT. Top (left to right): CT, PET, and fusion imaging in a 46-year-old man; the diagnosis was made by PET and CT. Bottom (left to right): CT, PET, and fusion imaging in a 63-year-old man; the diagnosis was made by PET only.

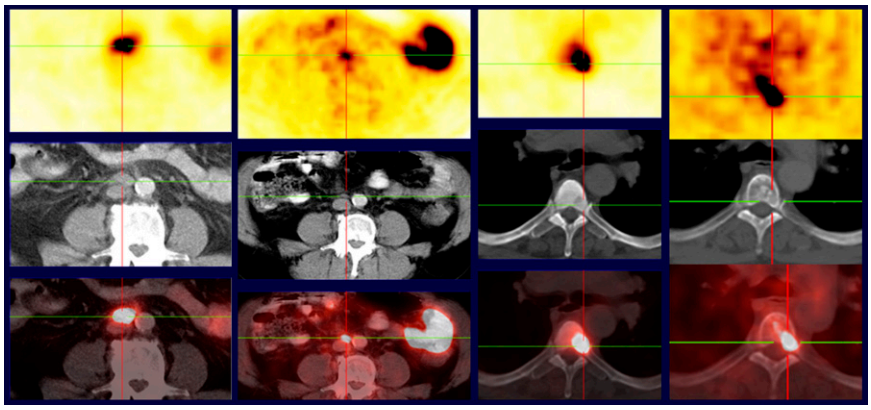

FIGURE 34. Examples of ^{68}Ga-PSMA-HBED-CC imaging in ^{177}Lu-PSMA-TUM1 therapy for prostate cancer. Left block of images acquired before (left column) and after (right column) therapy shows a significant decrease (89%) in SUV_{max} in the target lesion (paraaortic lymph node metastasis). Right block of images acquired before (left column) and after (right column) therapy shows a significant decrease (78%) in SUV_{max} in the target lesion (T5 vertebra).

Eiber et al. from the Technische Universität München (Germany) reported on "Evaluation of the detection rate for a novel ^{68}Ga-PSMA PET-ligand in patients with biochemical recurrence of prostate cancer using PET/CT and PET/MR imaging" [13]. The researchers showed in this cohort of 332 patients (256 with PET/CT, 76 with PET/MR) that the gallium-labeled PSMA agent showed more lesions than morphological imaging, including >80% detection on a per patient basis with PSA >1. It is interesting to note that in many of these cases, anatomic/morphologic imaging added only a small additional benefit (2.71%), although this additional percentage rose in cases in which PSA was very low (0.2–0.5). Anatomic imaging is clearly a positive addition, but many PET agents seem to find most of the disease, especially in the "golden" area of PSA <1 or <2 in which targeted radiotherapy is most effective. Figure 33 is an example showing disease with both PET and CT and with the PSMA-targeted agent.

Kulkarni et al. from the Zentralklinik Bad Berka (Germany) and the Technische Universität München (Germany) reported on "First clinical results with Lu-177 PSMA-TUM1 for the treatment of castrate-resistant metastatic prostate cancer" [10]. These authors showed uptake of ^{177}Lu-PSMA-TUM1 on posttherapy planar and SPECT imaging. Response evaluation by ^{68}Ga-PSMA-HBED-CC PET/CT showed excellent treatment response (partial remission), with decreases in target lesion SUV_{max} by 51% and 89% and disappearance of many of the previously noted PSMA-positive metastases in two patients (Figs. 34). This is another PSMA agent that is not only potentially beneficial for diagnosis but may also be a good radiotherapeutic.

Savir-Baruch et al. from Emory University (Atlanta, GA) and Columbia University (New York, NY) reported on "Diagnostic performance of synthetic amino acid anti-3-[^{18}F] FACBC PET in recurrent prostate carcinoma utilizing single-time versus dual-timepoint criteria" [21]. This group sought to address lack of specificity resulting from inflammation by using dual-timepoint imaging. They found very

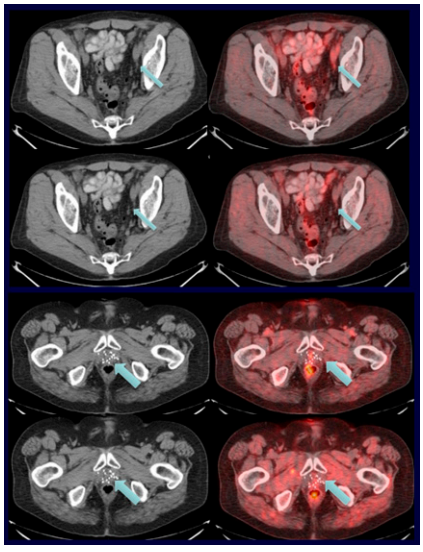

FIGURE 35. Single- vs dual-time-point criteria with synthetic amino acid anti-3-^{18}F-FACBC PET. Top: left external iliac lymph node with SUV_{max}/marrow SUV_{mean} >1 at 4 minutes (top row) and <1 at 17 minutes (next row) was defined as negative (true-negative) using dual time criteria. With early timepoint read criteria, the lymph node would have been misclassified as positive (false-positive). Bottom: midprostate SUV_{max}/marrow SUV_{mean} was >1 at 4 minutes (top row) and 17 minutes (bottom row) but was defined as negative given the decreased uptake and absence of focal uptake on delayed images (true-negative). With single-timepoint midprostate imaging this would have been misclassified as positive (false-positive).

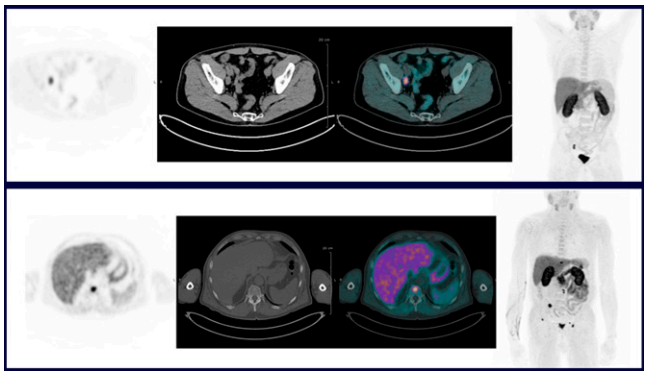

FIGURE 36. ^{18}F-choline PET/CT in biochemical recurrent prostate cancer. Example images highlight nodal uptake reflecting a metastatic focus (top panel), and an osseous metastasis to a vertebral body with a high degree of uptake (lower panel). The level of uptake contributes to a combined score reflecting the likelihood of progression free survival.

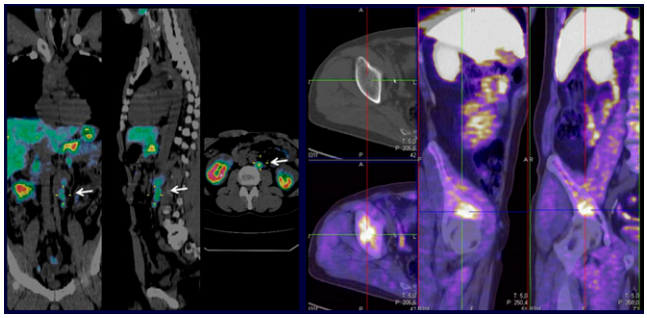

FIGURE 37. ^{18}F-fluorocholine PET/CT is more likely positive with a higher Gleason score of primary tumor. Example images. Left: lumbar lymph node recurrences in a patient treated with radical prostatectomy and lymphadenectomy (Gleason score, 10; PSA = 0.24 ng/mL). Right: osteomedullary lesion in the right ischium in a patient candidate for adjuvant radiotherapy (Gleason score, 9, PSA = 0.47 ng/mL).

little loss of sensitivity with dual-timepoint ^{18}F-FACBC PET imaging, but it helped to improve specificity (Fig. 35). As these agents continue to develop, we will need to look not only at outcomes but at factors such as specificity to address the issue of unnecessary biopsies. I believe that studies such as these are a step in the right direction in determining ways in which we can maximize not only the sensitivity but the specificity of these agents.

Pinaquy et al. from Centre Hospitalier Universitaire–Bordeaux (France) reported on "Comparative effectiveness of [^{18}F]-fluorocholine PET-CT and pelvic MRI with diffusion-weighted imaging (DWI) in the primary and lymph node staging of high-risk prostate cancer: Data from 47 prospectively enrolled patients" [399]. Sensitivity and specificity with ^{18}F-choline PET were 91% and 44%, respectively; for MR with DWI, these figures were 72% and 69%, respectively. For locoregional disease, sensitivity was lower for PET than for MR imaging (36% and 73%, respectively), a difference that was especially marked for seminal vesicle invasion. This suggests potential avantages for combining PET and MR for some prostate cancer imaging settings.

Colombié et al. from the Institut de Cancerologie de l'Ouest (ICO; Nantes, France), Urologic Clinica Nantes–Atlantis (Saint Herblain, France), and ICO/INSERM (Nantes, France) reported on "Prognostic value of metabolic parameters assessed by ^{18}F-choline PET/CT in biochemical recurrent prostate cancer: A retrospective study of 200 patients" [401]. Figure 36 is an example image from this study showing sites of recurrent disease. The authors performed a multivariate analysis with 3 simple criteria, age, standardized added metabolic activity, and SUV_{mean}, combined to create a prognostic score of 0–3. The resulting scores correlated well with progression-free survival. Our patients, of course, want to have some idea of the likelihood of progression-free survival. The cardiovascular literature, for example, has established good physician support for this information. This study is an example of the ways in which we are acquiring similar tools in molecular imaging and therapy that are helpful in patient guidance in oncology.

Evangelista et al. from the Oncological Institute of Veneto (Padua, Italy), National Cancer Institute (Aviano, Italy), and University Medical Center (Ljubljana, Slovenia) reported on "Detection of prostate cancer recurrence with ^{18}F-fluorocholine PET/CT in relation to Gleason score of primary tumor: experience on 1,000 patients" [398]. These authors found that in cases of suspected prostate cancer recurrence, a high Gleason score at the time of diagnosis was associated with a higher rate of positive ^{18}F-fluorocholine PET/CT scans, for each serum PSA level group at the time of imaging. It will be interesting to see whether and how PSMA agents or other amino acid agents correlate with these results. Figure 37 shows examples from this study.

Conclusion

Much ground was covered very rapidly in reviewing a selection of the oncologic presentations at the SNMMI meeting. It is clear that much original and exciting research is underway, much of it pointing toward the possibility of extraordinary future benefits in imaging and therapy for our patients.

Umar Mahmood, MD, PhD
Massachusetts General Hospital
Boston, MA